HHS Public Access

Author manuscript

Dev Cell. Author manuscript; available in PMC 2023 April 25.

Published in final edited form as:

Dev Cell. 2022 April 25; 57(8): 1009–1023.e5. doi:10.1016/j.devcel.2022.03.009.

Visceral mesoderm signaling regulates assembly position and function of the *Drosophila* testis niche

Lauren Anllo[1], **Stephen DiNardo**[1,2,*]

[1]Department of Cell and Developmental Biology, Perelman School of Medicine at the University of Pennsylvania, The Penn Institute for Regenerative Medicine, Philadelphia, PA 19104, USA

[2]Lead contact

SUMMARY

Tissue homeostasis often requires a properly placed niche to support stem cells. Morphogenetic processes that position a niche are just being described. For the *Drosophila* testis, we recently showed that pro-niche cells, specified at disparate positions during early gonadogenesis, must assemble into one collective at the anterior of the gonad. We now find that Slit and FGF signals emanating from adjacent visceral mesoderm regulate assembly. In response to signaling, niche cells express *islet,* which we find is also required for niche assembly. Without signaling, niche cells specified furthest from the anterior are unable to migrate, remaining dispersed. The function of such niches is severely disrupted, with niche cells evading cell cycle quiescence, compromised in their ability to signal the incipient stem cell pool, and failing to orient stem cell divisions properly. Our work identifies both extrinsic signaling and intrinsic responses required for proper assembly and placement of the testis niche.

In brief

Anllo and DiNardo investigate the formation of a stem cell niche, the stem cell microenvironment, during tissue development. They elucidate signaling required to assemble a niche, show that proper assembly is required for niche function, and reveal how one tissue can influence the development of a niche in an adjacent tissue.

INTRODUCTION

Stem cells play a vital role in tissue repair and maintenance, and their loss is associated with degeneration. To maintain stem cells within any tissue, these cells must receive self-renewal signals, often from their resident niche, a microenvironment that supports and

*Correspondence: sdinardo@pennmedicine.upenn.edu.

AUTHOR CONTRIBUTIONS

Conceptualization, L.A. and S.D.; methodology, L.A. and S.D.; validation, L.A.; formal analysis, L.A.; investigation, L.A.; resources, S.D.; data curation, L.A. and S.D.; writing – original draft, L.A.; writing – review & editing, L.A. and S.D.; visualization, L.A.; supervision, S.D.; project administration, L.A. and S.D.; funding acquisition, L.A. and S.D.

DECLARATION OF INTERESTS

The authors declare no competing interests.

SUPPLEMENTAL INFORMATION

Supplemental information can be found online at https://doi.org/10.1016/j.devcel.2022.03.009.

directs stem cell behavior (Losick et al., 2011; Moore and Lemischka, 2006; Morrison and Spradling, 2008). Assembly of a niche is crucial for stem cell function, and positioning of the assembled niche in the appropriate location during organ development ensures that niche signals remain accessible and confined to stem cells. Regulation of niche assembly and position are therefore relevant to tissue homeostasis. Morphogenetic and signaling events that underlie formation of tissues, where stem cells reside are being described in tissues such as the intestinal crypt and hair follicle (Greicius and Virshup, 2019; Kaestner, 2019; Martino et al., 2021; Rompalos and Greco, 2014; Shwartz et al., 2020). These tissues and others exhibit a paradigmatic compartmentalization of niche cells during organogenesis. However, how niche cells assemble in the appropriate position within their resident tissue remains largely unknown.

We study the *Drosophila* testis niche, which is well defined and has served as a paradigm for understanding niche-stem cell interactions. We refer to the testis niche, or niche cells, as the cells that emit signals to support neighboring stem cells. Our recent work pioneered live-imaging formation of this niche, enhancing its strength as a model (Anllo et al., 2019; Nelson et al., 2020). Appropriate placement of this niche is important for polarizing the testis and enabling tissue function (Fuller, 1993; Lee et al., 2008; Tanentzapf et al., 2007). The niche resides at the apex of a closed tube and directs germline stem cell (GSC) divisions such that some daughter cells are displaced from self-renewal signals. This arrangement facilitates the movement of differentiating cells further along the tube to eventually release mature sperm at the base (Fuller, 1993; Hardy et al., 1979; Kiger et al., 2001; Tulina and Matunis, 2001; Yamashita et al., 2003, 2007). Anchorage of the niche at the testis apex ensures proper niche positioning throughout the life of the fly. Without anchoring, the niche drifts from the apex, fails to properly orient divisions, and is eventually lost (Lee et al., 2008; Papagiannouli et al., 2014; Tanentzapf et al., 2007). Additionally, flies with defects in niche anchoring have reduced fertility (Lee et al., 2008), confirming the importance of niche position in testis function. Although we have some knowledge of how niche positioning is maintained, how the niche is initially assembled in its correct position is unknown and is the focus here (Anllo et al., 2019; Lee et al., 2008; Papagiannouli et al., 2014; Tanentzapf et al., 2007).

The niche assembles at the gonad anterior during embryonic development in the male (Aboim, 1945; Le Bras and Van Doren, 2006; Sheng et al., 2009; Sinden et al., 2012). The gonad is spherical and composed of germ cells (GCs) intermingled with and encysted by somatic gonadal precursor cells (SGPs) (Aboim, 1945; Jenkins et al., 2003). Prior to niche formation, prospective (pro) niche cells are specified from a subset of SGPs by coordination of Notch and EGFR signaling (Kitadate and Kobayashi, 2010; Okegbe and DiNardo, 2011). Once specified, pro-niche cells undergo two phases of niche morphogenesis, namely a loose assembly as a cap at the gonad anterior, followed by compaction into a tight, spherical structure (Anllo et al., 2019; Le Bras and Van Doren, 2006). The process by which pro-niche cells assemble at the anterior is dynamic. Pro-niche cells are initially intermingled with GCs. They extend protrusions to pull themselves onto the gonad periphery and then migrate anteriorly along extracellular matrix (ECM) until they associate in a cap (Anllo et al., 2019). This cap assembles at a pole directly opposite a group of male specific somatic gonadal precursor cells (msSGPs), located at the gonad posterior (Anllo et al., 2019; DeFalco

et al., 2003). Once assembled at the anterior, the niche displays distinguishing markers of adhesion and gene expression including Fasciclin III (Fas3), E-cadherin (Ecad), and *unpaired* (*upd*) (Le Bras and Van Doren, 2006). Niche morphogenesis is complete at the end of embryogenesis, Stage 17, and this arrangement is preserved through development, compartmentalizing the niche to the tip of the adult testis (Anllo et al., 2019; Sheng and Matunis, 2011; Sinden et al., 2012; Tanentzapf et al., 2007).

Our previous imaging showed that as niche assembly occurs the position adopted is tilted toward interior regions of the embryo (Anllo et al., 2019). The tilt suggested that tissues external to the gonad might be signaling to direct niche placement. The midgut is one tissue located near the assembled niche (Anllo et al., 2019). The midgut is surrounded by musculature derived from visceral mesoderm (Vm), and prior work suggested that Vm is a signaling center directing morphogenesis of the endoderm, salivary glands, and longitudinal visceral muscles (Azpiazu and Frasch, 1993; Bradley et al., 2003; Cimbora and Sakonju, 1995; Immerglück et al., 1990; Kadam et al., 2012; Tepass and Hartenstein, 1994). We thus suspected that the Vm could direct anterior assembly of the gonad niche.

Most of the Vm derives from segmentally repeated groups of mesodermal cells along the anterior-posterior axis of the embryo, specified by transcription factors including *bagpipe* and *biniou* (*bin*). After specification, Vm precursors contact one another in lateral arrangements on either side of the endoderm (Azpiazu and Frasch, 1993; Zaffran et al., 2001). Vm cells undergo fusion to form the circular muscles that later surround the gut and direct its morphogenesis (Immerglück et al., 1990; Klapper et al., 2002; Martin et al., 2001; Tepass and Hartenstein, 1994). Longitudinal muscles overlay the circular muscles and derive from caudal visceral mesoderm (cvm) precursors specified at the embryo posterior that migrate anteriorly over the Vm (Zaffran et al., 2001). Collectively, Vm tissue is known to express numerous signals, including Slit and FGFs. Slit activates Robo receptors, which act in cell adhesion and axon guidance during development. The FGFs Pyramus (Pyr) and Thisbe (Ths) activate the FGF receptor Heartless (Htl), which is important for guiding migration of cvm precursors over trunk Vm (Stathopoulos et al., 2004).

We reveal that Vm signals Slit and FGF are required to assemble a compartmentalized niche in the gonad. These signals are required for niche cell cytoskeletal polarity and anterior movement of pro-niche cells. In response to these signals, niche cells express the transcription factor *islet* (or *tup*), which is important for expression of axon guidance receptors in the nervous system (Santiago and Bashaw, 2014; Santiago and Bashaw, 2017; Yang et al., 2009). We demonstrate that Islet is also required to assemble the niche. Finally, we show that anterior niche assembly is important for proper niche function and behavior. Taken together, this work unveils how niche position arises during development.

RESULTS

Visceral mesoderm is required for niche assembly and positioning

To test for a role of the Vm in positioning the niche, we examined gonads dissected from *biniou* mutant embryos, which lack Vm tissue. *biniou* encodes a FoxF transcription factor essential for Vm development, with expression reported solely in Vm precursors

(Azpiazu and Frasch, 1993; Zaffran et al., 2001). In sibling controls dissected at the end of embryogenesis, Stage 17, when niche morphogenesis is normally complete, we observed a single anterior niche using both Fas3, a cell adhesion marker for niche cell boundaries, and *upd* > GFP, a marker for niche cell-specific gene expression (Figures 1A and 1C). Anterior niche position was confirmed relative to msSGPs at the gonad posterior. In contrast, gonads from *biniou* mutants often exhibited dispersed aggregates of niche cells (Figures 1B and 1D–1F). To rule out changes in the number of niche cells specified, we quantified niche and other SGPs and observed no differences between *biniou* mutant gonads and sibling controls (Figure 1G). Thus, the dispersed niche phenotype in *biniou* mutants results from defects in niche assembly. These data indicate that *biniou* is required for anterior niche assembly, which in turn suggests that the Vm is required to position the niche.

Visceral mesoderm tissue is required before niche assembly

To investigate the timing of the requirement, we examined *jelly belly* (*jeb*) mutants in which Vm cells are initially specified but do not complete development, and the Vm is missing by Stage 15 (Stute et al., 2004; Weiss et al., 2001). Stage 15 is the embryonic stage when niche assembly begins. Interestingly, *jeb* mutants had a normal number of niche cells and normal niche morphology (Figure 1H; data not shown). This result, along with the lack of proper niche assembly in *biniou* mutants suggests that the Vm is necessary early and dispensable by the time the niche assembles. Consistent with this, we also observed that at early stages prior to niche assembly, Vm precursor cells were intermingled with SGPs (Figure 1I). Such intermingling was also seen in *jeb* mutants (Figure 1J). In contrast, in *biniou* mutants we never observed intermingling of SGPs with the rare Vm precursors (Figure S1). These findings imply that Vm signals are active before commencement of niche assembly and may well involve direct cell contact between pro-niche and Vm cells.

Slit and the FGF ligands *pyr* and *ths* promote anterior niche assembly

biniou was reported to be expressed only in Vm and only to affect its development (Zaffran et al., 2001). However, we observed Biniou protein in SGPs in coalesced gonads (Figure S2). We thus sought to confirm a role for the Vm in niche assembly by mining existing literature for Vm-expressed genes that encoded ligands. The two FGF ligands–*pyramus* (pyr) and *thisbe* (*ths*), which often act redundantly–met these criteria (Kadam et al., 2012; Stathopoulos et al., 2004). We confirmed that each was expressed in Vm cells in Stages 13 and 16, before and during niche assembly, respectively (Figures S3A, S3B, S3D, and S3E). We observed expression in some other mesodermal cells outside the gonad, but not in the region where SGPs are located, interspersed among germline cells. In embryos where both *pyr* and *ths* were removed, gonadal niche cells were often dispersed or assembled but not located at the gonad anterior (Figures 2B, 2C, and 2E). A subset of Vm cells, the cvm, is missing in *pyr* and *ths* mutants, raising a possibility that these Vm ligands might act indirectly, through cvm, rather than directly in positioning the niche. However, niche placement is normal in a mutant lacking cvm (Figures S4E and S4F). In fact, consistent with a direct ligand requirement in positioning the niche, we observed expression of the Heartless FGF receptor in SGPs (Figures S4C and S4D), and *Htl* mutants also exhibited niche assembly defects (Figure 2F). These results demonstrate that the FGF ligands *pyr* and *ths* are important for assembling an anterior niche and could emanate from the Vm to do so.

The ligand Slit is expressed in Vm before and during niche assembly (Figures S3C and S3F; Kraut and Zinn, 2004; Rothberg et al., 1990; Sandmann et al., 2006; Soplop et al., 2012). We also detected occasional expression in other mesodermal cells, some of which flank the forming gonad but were not interspersed among GCs, and thus not SGPs (Figures S3C and S3F). We next examined *slit* mutants, which were previously shown to have a partially penetrant defect during an earlier phase of gonad development (Weyers et al., 2011). For that reason, we only analyzed that fraction of *slit* mutant gonads that formed properly, having bypassed the earlier role for Slit. In this manner, we ensured that any effects on niche morphology were unlikely to be secondary to some block in proper gonad formation. Indeed, we observed niche assembly defects in up to 40% of such *slit* mutant gonads (Figures 2D and 2G). Consistent with a role for Slit, the Slit receptors Robo1 and Robo2 have been observed in SGPs (Weyers et al., 2011), and we detected niche morphogenesis defects in *robo1* and *robo2* double mutants (Figure 2H; Figures S4G and S4H). These data support the idea that Slit, which is expressed in the Vm, contributes to proper assembly of an anterior gonad niche.

Since the removal of either Slit or the pair of FGF ligands resulted in a partial phenotype, we hypothesized that each of these pathways might independently contribute to niche assembly. Indeed, simultaneously removing Slit and both FGF ligands resulted in a virtually fully penetrant niche assembly defect (compare Figures 2I and 2J with Figures 2E and 2G). These data indicate that FGF and Slit act in parallel to facilitate the niche assembly. Finally, we also observed defects in gonads from embryos heterozygous for *slit*, *pyr*, and *ths* (Figures S4I–S4K), suggesting that the dosage of signaling ligands is relevant for proper niche assembly. To summarize, mutants for *biniou*, which have no Vm, exhibit niche assembly defects, and the removal of two classes of signaling ligands, which each appear to emanate from the Vm, exhibit virtually identical niche assembly defects. We conclude that the Vm is the main tissue responsible for assembling the gonadal niche in its correct position.

Slit and FGF ligands usually direct migratory paths during morphogenesis. To test whether these ligands might be playing a directional role for niche assembly, we misexpressed each ligand broadly in mesoderm and asked if that changed the position of niche assembly. Unfortunately, as seen before, *ths* or *pyr* overexpression led to general morphogenetic defects and impeded gonad formation such that no conclusion could be drawn (data not shown) (Sun and Stathopoulos, 2018). In contrast, *slit* overexpression occasionally yielded properly formed gonads. As with *slit* mutants, we only analyzed niche morphology where there was a properly coalesced gonad to ensure that any effects on the niche were not secondary to some block to gonad formation. Surprisingly, niche morphogenesis was unaffected by Slit overexpression when compared with siblings (Figure 2K), suggesting that Slit is acting as a competence factor and not a directional cue for niche assembly. Interestingly, GFP-tagged Slit appeared to accumulate at the gonad periphery, likely in the ECM (Figure S3G). This unpolarized accumulation could be consistent with the idea that Slit is not a directional cue.

Visceral mesoderm is required for anterior movement of pro-niche cells

We showed previously that proper niche assembly involves several steps, the first of which necessitates that pro-niche cells sort out of the internal milieu and onto the gonad periphery (Anllo et al., 2019). Signals from the Vm are not required for this step as niche cells in both control and *biniou* mutants were located at the gonad periphery to a similar degree (Figure 3G).

The second step of assembly requires anterior migration of pro-niche cells along the gonad periphery. A properly assembled niche is composed of some cells that were initially specified near their final position since they derive from parasegment (PS) 10 and other cells that were specified more centrally and thus must migrate anteriorly as revealed by lineage tracing PS 11 cells (Anllo et al., 2019; DeFalco et al., 2008; Le Bras and Van Doren, 2006). After assembly, lineage-traced PS 11 niche cells labeled with mcd8GFP (magenta) and Fas3 (green), whereas PS 10 cells only labeled with Fas3 (green; Figure 3A, arrow; Figure 3B). When we lineage-traced PS 11 cells in *biniou* mutants, most PS 11 niche cells remained in their original, more central positions and were less frequently associated with PS 10 niche cells (Figures 3C–3F). Since in the absence of Vm, PS 11-derived niche cells failed to reach the gonad anterior, and this suggests a requirement for Vm signaling during the second step of niche assembly.

Vm signaling results in *islet* expression in niche cells

Given the migratory steps in assembly, our prior finding of dispersed niches in gonads from *islet* (*tup*) mutants is revealing (Anllo et al., 2019; Figures 4A–4C), especially in light of its phenotypic similarity to *biniou* mutants and combined *slit*, *pyr*, and *ths* mutant (Figures 1 and 2). In fact, Islet protein was significantly enriched in niche cells (Figures 4E, S5A, and S5B), and a minimal element from the *islet* enhancer region (Bataillé et al., 2020; Boukhatmi et al., 2014) was sufficient to drive GFP expression in niche cells (Figure 4D). Moreover, Islet protein accumulation de pended on *biniou* (Figures S5C and S5D) and on slit, or pyr and *ths* (Figures 4F–4I). These results indicate that Slit and FGF signals, likely emanating from the Vm, act via *islet* to impact niche assembly.

Niche cells exhibit cytoskeletal polarity during assembly in response to Vm signaling

Since the cellular cytoskeleton is often polarized during migration, we examined the localization of F-actin during the later steps of niche assembly. Live imaging revealed enrichment along niche-niche interfaces, as these cells began to associate with one another at the gonad anterior (Figure 5A, 0 min). Interestingly, F-actin then repolarized to niche-GSC boundaries as assembly completed (Figure 5A, 50 min). Quantification in fixed tissue confirmed F-actin polarization during assembly (Figure 5B) and the shift afterward (Figure 5C). Thus, niche cell cytoskeletal polarity is regulated during assembly.

Recognizing that islet encodes a transcription factor that regulates adhesion and guidance in the nervous system (Santiago and Bashaw, 2014, 2017), we tested whether the cytoskeletal polarity observed for niche cells was disrupted in *islet* mutants. By quantifying polarity in mutants where niche cells had begun to associate with one another but had not completed assembly, we found that F-actin was not polarized (Figures 5D and 5E). Taken together, our

results suggest that Vm signals, Slit and FGF, regulate *islet* expression in the niche, which impacts polarization of the F-actin cytoskeleton and also promotes assembly (Figure 5F).

Once formed, it is known that the niche is enriched for cytoskeletal and adhesion proteins (Anllo et al., 2019; Le Bras and Van Doren, 2006). This prompted us to ask whether these components were polarized once assembly was completed. Indeed, both F-actin and E-cadherin were polarized, with F-actin enriched along niche-GSC interfaces compared with niche-niche interfaces, and E-cadherin enriched reciprocally, along niche-niche interfaces (Figures 5G–5J). Interestingly, in Stage 17, gonads from *biniou* mutants, neither F-actin nor E-cadherin, were polarized in niche cells (Figures 5K and 5L). Similarly, gonads from *fgf* or *slit* mutants also failed to polarize E-cadherin (Figures 5M and 5N; F-actin not assessed). These correlations suggest that without Vm signaling, any associations among niche cells that do occur are not organized properly.

Without Vm signaling, niche cells are functionally compromised and evade quiescence

We next tested whether niche assembly affected stem cell regulation. In the newly formed gonad, the niche recruits nearby GCs to adopt stem cell fate and orients stem cell divisions (Greenspan and Matunis, 2018; Hardy et al., 1979; Sheng et al., 2009; Sinden et al., 2012; Tanentzapf et al., 2007; Voog et al., 2008). One key niche-delivered signal, Upd, is known to activate the Stat pathway to higher levels among the first tier of germline cells adjacent to the niche (Anllo et al., 2019; Kiger et al., 2001; Leatherman and DiNardo, 2008, 2010; Sheng et al., 2009; Tulina and Matunis, 2001). We detected *upd* expression in niche cells in gonads from both control animals and *biniou* mutants (Figures 1C and 1D). As expected, in control gonads, Stat protein was enriched in presumptive GSCs relative to neighboring GCs (Figures 6A, 6A′, and 6C). In contrast, Stat enrichment was largely lost in gonads from *biniou* mutants and from double mutants when *slit* and the *pyr* and *ths* fgf ligands were removed (Figures 6B, 6B′, and 6C). These data suggest strongly that signaling from Vm affects niche function and that a properly assembled niche might be required for robust signaling to the stem cells.

Another key aspect of this niche is that it imposes oriented divisions on GSCs, such that daughter cells are displaced from the niche (Yamashita et al., 2003, 2007). In wild-type testes, signals from the niche orient divisions perpendicular to the niche-GSC interface (Chen et al., 2018). To accomplish this orientation, one centrosome in the GSC remains near the interface with the niche, whereas the duplicated centrosome moves to the opposite pole of the GSC (Sheng et al., 2009; Yamashita et al., 2003; Figure 6E). In contrast, in gonads from *biniou* mutants, both centrosomes in GSCs were often displaced from the interface with the nearby niche cell, suggesting a defect in centrosome anchoring (Figures 6D and 6F). These data again suggest functional defects in the niche in the absence of its proper assembly.

Strongly coupled to normal function of this niche is its quiescent state with respect to cell cycling (Greenspan and Matunis, 2018; Hetie and Cuevas, 2014). Indeed, EdU pulse-labeling showed that normal niche cells were quiescent (Figures 6G and 6I). In contrast, gonads with niche assembly defects exhibited many cycling niche cells (Figures 6H and 6I).

This defect was selective in that the S-phase index for GSCs was similar to controls (Figure 6J). Thus, without proper assembly, pro-niche cells fail to adopt their quiescent state.

Taken together, these results show defective niche signaling and behavior in the absence of Vm assembly cues, revealing that proper assembly is crucial to niche function.

DISCUSSION

We have shown that merely specifying niche cells is not sufficient for that niche to function. To adequately direct stem cell behavior, niche cells must be organized and positioned appropriately in the tissue. Prior live imaging suggested that niche placement was not simply congruent with the embryonic axes, but rather offset, tilted internally (Anllo et al., 2019). Here, we reveal the Vm as the likely tissue required for that precision in niche placement, and we identify signals expressed in Vm that govern this process. We show that those signals are delivered early in gonadogenesis and that in response, niche cells express the transcription factor *islet*, which plays a role in coordinating F-actin polarity in cells as they assemble into a niche that is functional and quiescent (see Figure 5F). Thus, this work identifies signaling, gene expression, and cell biological responses involved in regulating the assembly and proper positioning of the testis niche.

Visceral mesoderm regulates development of the testis niche

We observed a striking dispersed niche phenotype in the absence of the transcription factor *biniou*. *biniou* is essential for the formation of Vm, and its expression had been reported as exclusive to the Vm (Zaffran et al., 2001). However, we observe *Biniou* accumulation in both the Vm and in gonadal SGPs (Figure S2). Although this raised the possibility that Binou acted within SGPs, we identified two classes of ligands expressed in Vm, but not in SGPs, that impact niche development in a manner similar to *biniou*. We also ruled out the possibility that the ligands control niche assembly by regulating *biniou* in SGPs because SGP accumulation of *Biniou* was unaffected in mutants where all ligands were removed (Figure S2). These data strongly suggest that the Vm directs anterior niche assembly.

The Vm and its signals appear to affect a specific step of niche assembly. We recently showed that pro-niche cells first extend protrusions to pull themselves out to the gonad periphery, then move anteriorly to associate and form an anterior cap on the gonad (Anllo et al., 2019). In *biniou* mutants, niche cells get to the periphery, but a subset of these cells cannot successfully arrive anteriorly (Figure 3). Niche cells derive from two separate clusters of mesodermal cells that only later associate as one niche (DeFalco et al., 2008; Le Bras and Van Doren, 2006). Pro-niche cells specified in PS 10 mesoderm are already located at what will be the gonad anterior, whereas those specified in PS 11 must migrate to reach the anterior. The lack of proper assembly without Vm signaling suggests either that pro-niche cells cannot associate properly or migrate. Our data suggest the latter. Without either *biniou* or the ligands Slit and FGF, we find that pro-niche cells can still contact one another, likely as a result of sorting as niche cells upregulate adhesion proteins such as Fasciclin3, and E- and N-cadherins (Le Bras and Van Doren, 2006). However, our lineage tracing in *biniou* mutants revealed that PS 11-derived niche cells were almost never located at the gonad anterior (Figure 3E). We hypothesize that pro-niche cells specified in different

gonadal regions are not close enough to sort based on adhesion alone and require Vm signals to enable movement to form a single niche. Note that Vm signals also act on PS10 niche cells as Islet is expressed in all niche cells and expression is lost in the absence of Vm signals.

Vm signals are sent well before niche assembly

In many examples of cell migration, directive signals are active during the morphogenetic event (Montell, 2003; Scarpa and Mayor, 2016). We were surprised to find that the niche assembled normally in embryos that initially have Vm precursors but lose them prior to that time when the niche forms (Figure 1). From these data, we infer that Vm precursors emit the required signals early, significantly before niche assembly. One possibility is that early signaling induces a gene expression program in pro-niche cells that enables an appropriate intrinsic cell response later in gonadogenesis. Indeed, we showed that before niche assembly, pro-niche cells and Vm precursors directly intermingle and that *islet* gene expression is required downstream of Vm signaling. The identification of an *islet* cis-regulatory element sufficient for expression in the niche will help elucidate the circuitry involved in this induction event and establish whether it is a direct response to the signals defined here. Additionally, since *islet* itself is essential in niche assembly, its downstream targets will be of interest. In neurons, targets such as the DCC or Frazzled (Fra) receptor act in directing axons to their appropriate locations (Santiago and Bashaw, 2017). Perhaps, such candidates might explain how *islet* induction contributes to niche assembly.

Both Slit and FGF signals contribute to niche assembly and position

Our work has identified two signaling pathways important for niche assembly, suggesting that resiliency is built into the niche assembly process. Although each pathway appears necessary for *islet* expression (Figure 4), which is important for niche assembly, the apparent dependence on signal dosage (Figures 2 and S4) and the fact that some niches can assemble in the absence of one pathway (see Figure 2) suggest that the pathways cooperate to ensure proper assembly and positioning. The contributions of Slit and FGF to niche assembly are reminiscent of the partially overlapping roles of EGFR and PVR in border cell migration during *Drosophila* oogenesis. The immediate downstream effectors of these pathways are unique; however, both EGFR and PVR converge on directing the migratory path of the border cells (Duchek et al., 2001).

In many cases, Slit and FGF function as directional guidance cues (Blockus and Chédotal, 2016; Friedl and Gilmour, 2009; Kadam et al., 2012). Changing the source of the cue in these instances alters the path of migrating cells (Jia et al., 2005; Sutherland et al., 1996). In niche assembly, we tested whether these pathways were acting in this manner. Although we could not analyze niche assembly upon FGF misexpression, *slit* misexpression did yield gonads with properly assembled and positioned niches (Figure 2K). This result argues that Slit is in fact not acting as a directional cue during niche assembly. Slit protein is known to accumulate in nearby ECM in other systems (Isaacman-Beck et al., 2015; Xiao et al., 2011), and we likewise detected Slit accumulation near gonadal ECM, surrounding the periphery of the gonad (Figure S3G). This apparently symmetric accumulation of Slit is consistent with our interpretation that Slit is not acting as a directional cue. Our data instead suggest that

Slit provides for "competence," acting, for example, to enable pro-niche cells to migrate, or licensing responses to as yet unidentified directional cues.

Slit and FGF signaling affects cytoskeletal organization in pro-niche cells

If Slit and FGF are eliciting responses prior to niche assembly, it is possible that they might regulate modulators of cell behavior required for assembly. Such regulators could be Islet targets. Cell movement often relies on asymmetric localization of cytoskeletal or adhesion proteins (Etienne-Manneville, 2008; Scarpa and Mayor, 2016; Vassilev et al., 2017). We showed that niche cytoskeletal polarity is normally well organized during late stages of assembly and that this organization is lost without *islet* (Figure 5). These data suggest that the niche assembly process depends on proper cytoskeletal polarization of pro-niche cells in response to Vm signaling.

Without proper assembly, niche cells function abnormally and evade quiescence

Niches are commonly found in a stereotypical position in each tissue. In mammals, the intestinal niche is within crypts and the dermal papillae niche assembles at the base of the hair follicle (Wang et al., 2016). Such reproducibility in the organization of niche cells suggests that proper niche assembly might be linked to its function, and our work reveals evidence of this link. We show that proper assembly of the testis niche is required to activate robust signaling in neighboring GCs and to orient stem cell divisions (Figures 6A–6F), two crucial outputs of niche signaling. In the adult testis, both of these outputs have been linked to intimate, cell biological organization at niche-stem cell interfaces (Chen et al., 2018; Inaba et al., 2015; Michel et al., 2011). Further, niche cells normally exhibit cell cycle quiescence (Greenspan and Matunis, 2018; Hardy et al., 1979; Voog et al., 2008), although promoting division of adjacent stem cells (Yamashita et al., 2003). We reveal an association between initial niche assembly and quiescence. It is clear that quiescence is important to the biology of the testis, as aberrantly dividing niche cells can generate extraneous niches located away from the testis tip and even lead to niche decay (Greenspan and Matunis, 2018; Herrera et al., 2021). There is evidence for feedback from other adult somatic cells in maintaining niche quiescence, but how niche cells first enter quiescence is unknown. All embryonic SGPs are cycling prior to niche formation, but fully assembled niche cells withdraw from cycling (Figures 6G and 6I), and assembly appears correlated with withdrawal (Figures 6H and 6I). Whether and how niche-niche cell contact and the tight regulation of cytoskeletal organization during assembly, including the asymmetric enrichment of E-cadherin in assembled niches, is related to quiescence will require further study.

Together, our work identifies extrinsic signaling and intrinsic gene expression and cell biological responses involved in governing niche cellular organization and position, which are integral to proper function of the testis niche.

Limitations of the study

Although our overexpression experiments suggest that Slit is not acting as a directional guidance cue, these experiments were unable to determine whether FGF ligands were providing directional guidance, as overexpression of either the Pyr or Ths ligand precluded

gonad formation. Our Islet immunostaining experiments reveal that *islet* is expressed in response to both Slit and FGF; however, we have not discerned whether islet expression is a direct response to signaling. Future work will ask whether other key intermediaries are influencing *islet* in response to signaling. Finally, our work has not determined that *islet* expression is the only relevant niche cell response to extrinsic signaling. Expression is the only relevant niche cell response cell response to extrinsic signaling

STAR★METHODS

RESOURCE AVAILABILITY

Lead contact

- Further information and requests for resources and reagents should be directed to and will be fulfilled by the lead contact, Stephen DiNardo (sdinardo@pennmedicine.upenn.edu).

Materials availability

- This study did not generate new unique reagents.

Data and code availability

- All data reported in this paper will be shared by the lead contact upon request.
- This paper does not report original code.
- Any additional information required to reanalyze the data reported in this paper is available from the lead contact upon request.

EXPERIMENTAL MODEL AND SUBJECT DETAILS

***Drosophila* stocks—**All *Drosophila* lines used are listed in the key resources table (KRT). *slit[2]* is a null allele with no detectable protein product (Battye et al., 2001; Nusslein-Volhard et al., 1984). To remove *pyr* and *ths* together, we used a small chromosomal deficiency, Df(2R)BSC25, which completely deletes the genes encoding both ligands (Stathopoulos et al., 2004). *jeb[*weli*]* mutants lack visceral muscle founder cells (Stute et al., 2004), and the small chromosomal deficiency, Df(2R)BSC699 uncovers *jeb. hlh54f[delta598]* mutants lack caudal visceral mesoderm (Ismat et al., 2010). *htl[AB42]* is a null allele of the FGF receptor *heartless* (Gisselbrecht et al., 1996). *robo2[X123]* and *robo1[GA285]* are null alleles of the Slit receptors *robo2* and *robo1* (Evans et al., 2015; Kidd et al., 1998).

Sex identification and genotyping—Gonad sex identification was accomplished as described by Anllo and colleagues (Anllo et al., 2019). We used Vasa antibody staining to identify larger male gonads, and male specific SGPs (msSGPs). Vasa antibody labels both germ cells and msSGPs, and we identified msSGPs using Vasa antibody alongside a DNA stain to indicate small, Vasa positive nuclei. Sibling controls were distinguished from homozygous mutants by using fluorescent balancer chromosomes (TM3, P{w[+mC]=Gal4-twi.G}2.3, P{UAS-2xEGFP} AH2.3, Sb[1], Ser[1], FBst0006663; TM6, P{Dfd-EYFP}, Sb, Hu, e; or CyO, P{Dfd-EYFP}).

METHOD DETAILS

Embryonic gonad dissection and immunostaining—Dissections and immunostaining were performed as previously described (Anllo et al., 2019). Embryos were collected and aged 22–25 hours in a humidified chamber at 25 degrees C for late stage 17 embryos. For younger embryos still undergoing late stages of niche assembly, embryos were aged 22.5–24.5 hours at 23 degrees C. Primary antibodies were used overnight at 4 degrees C. Secondary antibodies were used at 3.75 ug/mL (Alexa488, Cy3, or Alexa647; Molecular Probes; Jackson ImmunoResearch) for 1–2 hr at room temperature. DNA was stained with Hoechst 33342 (Sigma) at 0.2 ug/mL for 5 min.

We used rabbit antibody against Vasa 1:5000 (gift from R. Lehmann, NYU), STAT92E 1:1000 (gift from E. Bach, NYU), and RFP 1:500 (Abcam, ab62341); goat antibody against Vasa 1:200 (Santa Cruz, dC-13, now discontinued); mouse antibody against Fasciclin III 1:50 (DSHB, 7G10), Islet 1.5:100 (DSHB 40.3A4; *Drosophila* Tailup), and Gamma Tubulin 1:200 (Sigma, GTU-88); rat antibody against DE-cadherin 1:20 (DSHB, DCAD2); guinea pig antibody against Traffic jam 1:10,000 (gift from D. Godt); chick antibody against GFP 1:1000 (Aves Labs, GFP-1020); and rabbit antibody against *Biniou* 1:100 (gift from E. Furlong). Images of fixed samples were acquired on a Zeiss Imager with Apotome using a 40x, 1.2 N.A. lens or a 20x, 0.8 N.A. lens; or on a Zeiss LSM 880 Confocal with Airyscan and Fast Airyscan, 40x, 1.2 N.A. lens.

Identification of niche position—To confirm the position of niche cells relative to the anterior-posterior axis of the gonad, we used the position of the male specific somatic gonadal precursor cells (msSGPs) to denote the gonad posterior (DeFalco et al., 2003). msSGPs are visible to a trained eye in many stains, and can be detected as a cluster of cells distinct from the germ cells at the posterior pole of the gonad with Vasa immunostaining (Anllo et al., 2019; Sheng et al., 2009). Because the embryonic gonad has a spherical shape, we confirmed an anteriorly positioned niche by its location at the pole of the gonad roughly 180 degrees opposite to where the msSGP cluster resides.

Niche phenotypic characterization—Normal niches were located in a single grouping of cells at the gonad anterior, with a smoothened boundary. Dispersed niches included a range of phenotypes, including cases where multiple distinct niche cell groupings were present within a single gonad, and cases where a single niche cell grouping formed with highly irregular boundaries.

***In vivo* live imaging—**Live imaging was performed as previously described (Anllo et al., 2019; Ong et al., 2019). Images were acquired with a Leica DM16000 B spinning disk confocal with a 63 ×1.2 N.A. water immersion objective, using an EMCCD camera (Andor iXon 3 897E or Hamamatsu photonics, model C9100-13) controlled by Metamorph software. Z stacks were taken at 5-minute intervals, with 36 1 um z-slices through the gonad.

Slit and FGF ligand overexpression—The *twi*-Gal4 driver was use to over-express either UAS-*sli.D* or UAS-*ths289.22* in all mesodermal cells. Embryos were collected for 2–3 hours at 29 degrees C, and were aged 15–18 hours at 29 degrees prior to dissection. Just

prior to dissection, UAS-eGFP expression was used to distinguish and sort embryos that carried the *twi*-Gal4 driver from sibling controls.

EdU pulse experiments—EdU pulse experiments were performed using the Click-iT EdU Plus kit (Molecular Probes, c10640) (Salic and Mitchison, 2008). Immediately after dissection, tissue was incubated in 10 uM EdU in *Drosophila* Ringers solution for 30 minutes at room temperature. Tissue was then fixed for 15 min in 4% PFA at room temperature. The azide reaction to couple EdU to alexa647 was performed either prior to, or after antibody staining. Copper catalyst was used at a concentration of 4 nM.

QUANTIFICATION AND STATISTICAL ANALYSIS

Counting niche cells—Niche cells were identified using the niche-cell specific Fasciclin III immunostain. Niche cell nuclei were counted, using either Hoechst DNA stain, or Traffic Jam nuclear stain, as a marker. The ImageJ Cell Counter plugin was used to record counted niche cells. A Mann-Whitney test was used to determine significance of $p < 0.05$.

Quantification of *islet* expression in *slit*, and *pyr* and ths removed (*fgf*) mutants—To quantify *islet* expression in Vm ligand mutants, we stained gonads with Islet antibody and used ImageJ to measure the mean gray value fluorescence intensity within regions of interest (ROIs). We selected ROIs including a circular region within somatic cell nuclear boundaries, using Hoechst stain as a marker. For each gonad, 3 niche cell ROIs were measured for Islet expression. An ROI devoid of tissue was selected in a region adjacent to the gonad to determine background fluorescence. Background fluorescence was subtracted from measured niche cell values. Each background-subtracted value was normalized to the mean Islet fluorescence for the gonad, measured at a Z slice including the niche. Mann-Whitney tests were used to determine significance of $p < 0.05$.

Quantification of *islet* expression in *biniou* mutants—To quantify *islet* expression in *biniou* mutants, we stained gonads with Islet antibody and used ImageJ to measure the mean gray value fluorescence intensity within regions of interest (ROIs). We selected ROIs including a circular region within somatic cell nuclear boundaries, using *six4*nlsGFP as a marker. ROIs were in a single Z plane in which the relevant nucleus was in focus. For each gonad, 3 niche cells and 3 non-niche SGP ROIs were measured for Cy3 Islet and for GFP nuclear marker fluorescence. An ROI selected to encompass the unlabeled region of a single germ cell within each gonad was used to determine background fluorescence. Background fluorescence was subtracted from measured values.

To control for possible bleed-through of GFP nuclear marker into the Cy3 Islet channel, we first measured the amount of Cy3 signal that could be accounted for by GFP bleed-through. We plotted the ratio of Cy3 to GFP fluorescence intensity in gonads that were not stained with Islet antibody, and thus should not have any Islet Cy3 signal. This plot determined that Cy3 signal resulting from bleed-through averaged 7% of the GFP signal intensity for each ROI. Thus, in addition to background subtraction, we also subtracted 7% of the GFP signal values from Cy3 values to obtain our final measurements of Cy3 Islet signal. These values were plotted. Mann-Whitney tests were used to determine significance of $p < 0.05$.

Quantification of normalized F actin and E-cadherin fluorescence—To visualize F actin we imaged gonads expressing a GFP-labeled F actin binding protein in the somatic cells, *six4*-eGFP::moesin (Sano et al., 2012). E-cadherin was visualized by immunostaining with an antibody against E-cadherin (DSHB). For all experiments, gonads were dissected and immunostained either with an antibody against GFP, or E-cadherin. Niche interfaces were identified with a Fas3 immunostain. F actin or E-cadherin fluorescence intensity at niche-niche and niche-GSC interfaces was quantified using ImageJ to trace interfaces, and report mean gray values. Background fluorescence was measured as the mean gray value of a line traced where no tissue was present for E-cadherin experiments, or within a germ cell for F actin, as germ cells do not express *six4*-eGFP::moesin. After background subtraction, fluorescence intensity was normalized by taking the ratio of each interface measurement to the average of all interfaces within that gonad. Normalized values were then plotted, and data was analyzed using a Mann-Whitney test.

Centrosome position quantification—Centrosome position was visualized with immunofluorescence against Gamma tubulin to label pericentriolar material. GSCs were scored for centrosome position if they had already undergone centrosome duplication. We quantified how often one of the two centrosomes was located closer to the adjacent niche than to other neighboring cells. Those GSCs with a centrosome located near the niche-GSC interface were scored as appropriately positioned. GSCs in Vm mutants often failed to maintain a centrosome near the niche. GSCs in Vm mutants that made contact with niche cells at multiple points around their periphery were scored as normal if a centrosome was close to one of these niche-GSC contacts. Data was analyzed using Fisher's exact test.

Quantification of Stat accumulation—To quantify Stat accumulation, we stained gonads with Stat antibody (E. Bach, 1:1000) and used ImageJ to measure the mean gray value fluorescence intensity within regions of interest (ROIs). We selected ROIs including a circular region to sample germ cells, using Vasa immunofluorescence as a marker to delineate cell boundaries. For each gonad, we sampled 5 GSCs and 3 neighboring germ cells. After background subtraction, we measured the ratio of Stat accumulation within each GSC relative to the neighboring germ cell average for that gonad. Relative Stat enrichment values were plotted for each GSC. We obtained measurements on sibling controls and in mutants for *biniou*, or for combined *slit* and *fgf*-removed mutants. Mann-Whitney tests were used to evaluate comparisons.

Supplementary Material

Refer to Web version on PubMed Central for supplementary material.

ACKNOWLEDGMENTS

We thank the Bloomington Drosophila Stock Center (NIH P40OD018537), director of our CDB microscopy core Andrea Stout, and R. Lehmann, E. Bach, A. Holz, and M. Frasch for antibodies and stocks. Thanks to G. Bashaw, M. Granato, K. Nelson, G. Vida, B. Warder, and especially K. Lenhart for comments. Work was supported by NIH grants GM125123 to L.A.; R01 GM60804, R33 AG047915, and R35 GM136270 to S.D.

REFERENCES

Aboim AN (1945). Development embryonnair et postembryonnair des gonads normale et agametiques de *Drosophila* melanogaster. Rev. Suisse Zool 53, 53–154.

Anllo L, Plasschaert LW, Sui J, and DiNardo S (2019). Live imaging reveals hub cell assembly and compaction dynamics during morphogenesis of the *Drosophila* testis niche. Dev. Biol 446, 102–118. [PubMed: 30553808]

Azpiazu N, and Frasch M (1993). Tinman and bagpipe: two homeo box genes that determine cell fates in the dorsal mesoderm of *Drosophila*. Genes Dev. 7, 1325–1340. [PubMed: 8101173]

Bataillé L, Colombié N, Pelletier A, Paululat A, Lebreton G, Carrier Y, Frendo J-L, and Vincent A (2020). Alary muscles and TARMs, a novel type of striated muscles maintaining internal organs positions. Development 147, dev185645. [PubMed: 32188630]

Battye R, Stevens A, Perry RL, and Jacobs JR (2001). Repellent signaling by slit requires the leucine-rich repeats. J. Neurosci 21, 4290–4298. [PubMed: 11404414]

Blockus H, and Chédotal A (2016). Slit-robo signaling. Development 143, 3037–3044. [PubMed: 27578174]

Boukhatmi H, Schaub C, Bataillé L, Reim I, Frendo JL, Frasch M, and Vincent A (2014). An Org-1—tup transcriptional cascade reveals different types of alary muscles connecting internal organs in *Drosophila*. Development 141, 3761–3771. [PubMed: 25209244]

Bradley PL, Myat MM, Comeaux CA, and Andrew DJ (2003). Posterior migration of the salivary gland requires an intact visceral mesoderm and integrin function. Dev. Biol 257, 249–262. [PubMed: 12729556]

Chen C, Cummings R, Mordovanakis A, Hunt AJ, Mayer M, Sept D, and Yamashita YM (2018). Cytokine receptor-EB1 interaction couples cell polarity and fate during asymmetric cell division. Elife 7, 1–19.

Cimbora DM, and Sakonju S (1995). *Drosophila* midgut morphogenesis requires the function of the segmentation gene odd-paired. Dev. Biol 169, 580–595. [PubMed: 7781900]

DeFalco T, Camara N, Le Bras S, and Van Doren M (2008). Nonautonomous sex determination controls sexually dimorphic development of the *Drosophila* Gonad. Dev. Cell 14, 275–286. [PubMed: 18267095]

DeFalco TJ, Verney G, Jenkins AB, McCaffery JM, Russell S, and Van Doren M (2003). Sex-specific apoptosis regulates sexual dimorphism in the *Drosophila* embryonic gonad. Dev. Cell 5, 205–216. [PubMed: 12919673]

Duchek P, Somogyi K, Jékely G, Beccari S, and Rørth P (2001). Guidance of cell migration by the *Drosophila* PDGF/VEGF receptor. Cell 107, 17–26. [PubMed: 11595182]

Etienne-Manneville S (2008). Polarity proteins in migration and invasion. Oncogene 27, 6970–6980. [PubMed: 19029938]

Evans TA, Santiago C, Arbeille E, and Bashaw GJ (2015). Robo2 acts in trans to inhibit slit-robo1 repulsion in pre-crossing commissural axons. Elife 4, e08407. [PubMed: 26186094]

Friedl P, and Gilmour D (2009). Collective cell migration in morphogenesis, regeneration and cancer. Nat. Rev. Mol. Cell Biol 10, 445–457. [PubMed: 19546857]

Fuller MT (1993). Spermatogenesis. In The Development of Drosophila melanogaster, Bate M and Martinez-Arias A, eds. (Cold Spring Harbor Labs Press).

Gisselbrecht S, Skeath JB, Doe CQ, and Michelson AM (1996). heartless encodes a fibroblast growth factor receptor (DFR1/DFGF-R2) involved in the directional migration of early mesodermal cells in the *Drosophila* embryo. Genes Dev. 10, 3003–3017. [PubMed: 8957001]

Greenspan LJ, and Matunis EL (2018). Retinoblastoma intrinsically regulates niche cell quiescence, identity, and niche number in the adult *Drosophila* testis. Cell Rep. 24, 3466–3476.e8. [PubMed: 30257208]

Greicius G, and Virshup DM (2019). Stromal control of intestinal development and the stem cell niche. Differentiation 108, 8–16. [PubMed: 30683451]

Hardy RW, Tokuyasu KT, Lindsley DL, and Garavito M (1979). The germinal proliferation center in the testis of *Drosophila melanogaster*. J. Ultrastruct. Res 69, 180–190. [PubMed: 114676]

Herrera SC, Sainz de la Maza D, Grmai L, Margolis S, Plessel R, Burel M, O'Connor M, Amoyel M, and Bach EA (2021). Proliferative stem cells maintain quiescence of their niche by secreting the activin inhibitor follistatin. Dev. Cell 56, 2284–2294.e6. [PubMed: 34363758]

Hetie P, de Cuevas M, and Matunis E (2014). Conversion of quiescent niche cells to somatic stem cells causes ectopic niche formation in the *Drosophila* testis. Cell Rep. 7, 715–721. [PubMed: 24746819]

Immerglück K, Lawrence PA, and Bienz M (1990). Induction across germ layers in *Drosophila* mediated by a genetic cascade. Cell 62, 261–268. [PubMed: 1973634]

Inaba M, Buszczak M, and Yamashita YM (2015). Nanotubes mediate niche-stem-cell signalling in the *Drosophila* testis. Nature 523, 329–332. [PubMed: 26131929]

Isaacman-Beck J, Schneider V, Franzini-Armstrong C, and Granato M (2015). The lh3 glycosyltransferase directs target-selective peripheral nerve regeneration. Neuron 88, 691–703. [PubMed: 26549330]

Ismat A, Schaub C, Reim I, Kirchner K, Schultheis D, and Frasch M (2010). HLH54F is required for the specification and migration of longitudinal gut muscle founders from the caudal mesoderm of *Drosophila*. Development 137, 3107–3117. [PubMed: 20736287]

Jenkins AB, Mccaffery JM, and Van Doren M (2003). *Drosophila* E-cadherin is essential for proper germ cell-soma interaction during gonad morphogenesis. Development 130, 4417–4426. [PubMed: 12900457]

Jia L, Cheng L, and Raper J (2005). Slit/Robo signaling is necessary to confine early neural crest cells to the ventral migratory pathway in the trunk. Dev. Biol 282, 411–421. [PubMed: 15950606]

Kadam S, Ghosh S, and Stathopoulos A (2012). Synchronous and symmetric migration of *Drosophila* caudal visceral mesoderm cells requires dual input by two FGF ligands. Development 139, 699–708. [PubMed: 22219352]

Kaestner KH (2019). The intestinal stem cell niche: a central role for Foxl1-expressing subepithelial telocytes. Cell. Mol. Gastroenterol. Hepatol 8, 111–117. [PubMed: 30965141]

Kidd T, Brose K, Mitchell KJ, Fetter RD, Tessier-Lavigne M, Goodman CS, and Tear G (1998). Roundabout controls axon crossing of the CNS midline and defines a novel subfamily of evolutionarily conserved guidance receptors. Cell 92, 205–215. [PubMed: 9458045]

Kiger AA, Jones DL, Schulz C, Rogers MB, and Fuller MT (2001). Stem cell self-renewal specified by JAK-STAT activation in response to a support cell cue. Science 294, 2542–2545. [PubMed: 11752574]

Kitadate Y, and Kobayashi S (2010). Notch and EGFR signaling act antagonistically to regulate germ-line stem cell niche formation in *Drosophila* male embryonic gonads. Proc. Natl. Acad. Sci. USA 107, 14241–14246. [PubMed: 20660750]

Klapper R, Stute C, Schomaker O, Strasser T, Janning W, Renkawitz-Pohl R, and Holz A (2002). The formation of syncytia within the visceral musculature of the *Drosophila* midgut is dependent on duf, sns and mbc. Mech. Dev 110, 85–96. [PubMed: 11744371]

Kraut R, and Zinn K (2004). Roundabout 2 regulates migration of sensory neurons by signaling in trans. Curr. Biol 14, 1319–1329. [PubMed: 15296748]

Le Bras S, and Van Doren M (2006). Development of the male germline stem cell niche in *Drosophila*. Dev. Biol 294, 92–103. [PubMed: 16566915]

Leatherman JL, and DiNardo S (2008). Zfh-1 controls somatic stem cell self-renewal in the *Drosophila* testis and nonautonomously influences germline stem cell self-renewal. Cell Stem Cell 3, 44–54. [PubMed: 18593558]

Leatherman JL, and DiNardo S (2010). Germline self-renewal requires cyst stem cells and stat regulates niche adhesion in *Drosophila* testes. Nat. Cell Biol 12, 806–811. [PubMed: 20622868]

Lee S, Zhou L, Kim J, Kalbfleisch S, and Schöck F (2008). Lasp anchors the *Drosophila* male stem cell niche and mediates spermatid individualization. Mech. Dev 125, 768–776. [PubMed: 18655828]

Losick VP, Morris LX, Fox DT, and Spradling A (2011). *Drosophila* stem cell niches: a decade of discovery suggests a unified view of stem cell regulation. Dev. Cell 21, 159–171. [PubMed: 21763616]

Martin BS, Ruiz-Gómez M, Landgraf M, and Bate M (2001). A distinct set of founders and fusion-competent myoblasts make visceral muscles in the *Drosophila* embryo. Development 128, 3331–3338. [PubMed: 11546749]

Martino PA, Heitman N, and Rendl M (2021). The dermal sheath: an emerging component of the hair follicle stem cell niche. Exp. Dermatol 30, 512–521. [PubMed: 33006790]

Michel M, Raabe I, Kupinski AP, Pérez-Palencia R, and Bökel C (2011). Local BMP receptor activation at adherens junctions in the *Drosophila* germ-line stem cell niche. Nat. Commun 2, 415. [PubMed: 21811244]

Montell DJ (2003). Border-cell migration: the race is on. Nat. Rev. Mol. Cell Biol 4, 13–24. [PubMed: 12511865]

Moore KA, and Lemischka IR (2006). Stem cells and their niches. Science 311, 1880–1885. [PubMed: 16574858]

Morrison SJ, and Spradling AC (2008). Stem cells and niches: mechanisms that promote stem cell maintenance throughout life. Cell 132, 598–611. [PubMed: 18295578]

Nelson KA, Warder BN, DiNardo S, and Anllo L (2020). Dissection and live-imaging of the late embryonic *Drosophila* gonad. J. Vis. Exp 164, 1–19.

Nusslein-Volhard C, Wieschaus E, and Kluding H (1984). Mutations affecting the pattern of the larval cuticle in *Drosophila* melanogaster. Wilhelm Rouxs Arch. Dev. Biol 193, 267–282.

Okegbe TC, and DiNardo S (2011). The endoderm specifies the mesodermal niche for the germline in *Drosophila* via Delta-Notch signaling. Development 138, 1259–1267. [PubMed: 21350008]

Ong K, Collier C, and DiNardo S (2019). Multiple feedback mechanisms fine-tune Rho signaling to regulate morphogenetic outcomes. J. Cell Sci 132, jcs224378. [PubMed: 30872456]

Papagiannouli F, Schardt L, Grajcarek J, Ha N, and Lohmann I (2014). The hox gene Abd-B controls stem cell niche function in the *Drosophila* testis. Dev. Cell 28, 189–202. [PubMed: 24480643]

Rompalos P, and Greco V (2014). Stem cell dynamics in the hair follicle niche. Semin. Cell Dev. Biol 25–26, 34–42.

Rothberg JM, Jacobs JR, Goodman CS, and Artavanis-Tsakonas S (1990). slit: an extracellular protein necessary for development of midline glia and commissural axon pathways contains both EGF and LRR domains. Genes Dev. 4, 2169–2187. [PubMed: 2176636]

Salic A, and Mitchison TJ (2008). A chemical method for fast and sensitive detection of DNA synthesis *in vivo*. Proc. Natl. Acad. Sci. USA 105, 2415–2420. [PubMed: 18272492]

Sandmann T, Jensen LJ, Jakobsen JS, Karzynski MM, Eichenlaub MP, Bork P, and Furlong EEM (2006). A temporal map of transcription factor activity: Mef2 directly regulates target genes at all stages of muscle development. Dev. Cell 10, 797–807. [PubMed: 16740481]

Sano H, Kunwar PS, Renault AD, Barbosa V, Clark IBN, Ishihara S, Sugimura K, and Lehmann R (2012). The *Drosophila* actin regulator ENABLED regulates cell shape and orientation during gonad morphogenesis. PLoS One 7, e52649. [PubMed: 23300733]

Santiago C, and Bashaw GJ (2014). Transcription factors and effectors that regulate neuronal morphology. Development 141, 4667–4680. [PubMed: 25468936]

Santiago C, and Bashaw GJ (2017). Islet coordinately regulates motor axon guidance and dendrite targeting through the frazzled/DCC receptor. Cell Rep. 18, 1646–1659. [PubMed: 28199838]

Scarpa E, and Mayor R (2016). Collective cell migration in development. J. Cell Biol 212, 143–155. [PubMed: 26783298]

Sheng XR, and Matunis E (2011). Live imaging of the *Drosophila* spermatogonial stem cell niche reveals novel mechanisms regulating germline stem cell output. Development 138, 3367–3376. [PubMed: 21752931]

Sheng XR, Posenau T, Gumulak-Smith JJ, Matunis E, Van Doren M, and Wawersik M (2009). Jak-STAT regulation of male germline stem cell establishment during *Drosophila* embryogenesis. Dev. Biol 334, 335–344. [PubMed: 19643104]

Shwartz Y, Gonzalez-Celeiro M, Chen CL, Pasolli HA, Sheu SH, Fan SMY, Shamsi F, Assaad S, Lin ETY, Zhang B, et al. (2020). Cell types promoting goosebumps form a niche to regulate hair follicle stem cells. Cell 182, 578–593.e19. [PubMed: 32679029]

Sinden D, Badgett M, Fry J, Jones T, Palmen R, Sheng X, Simmons A, Matunis E, and Wawersik M (2012). Jak-STAT regulation of cyst stem cell development in the *Drosophila* testis. Dev. Biol 372, 5–16. [PubMed: 23010510]

Soplop NH, Cheng YS, and Kramer SG (2012). Roundabout is required in the visceral mesoderm for proper microvillus length in the hindgut epithelium. Dev. Dyn 241, 759–769. [PubMed: 22334475]

Stathopoulos A, Tam B, Ronshaugen M, Frasch M, and Levine M (2004). pyramus and thisbe: FGF genes that pattern the mesoderm of *Drosophila* embryos. Genes Dev. 18, 687–699. [PubMed: 15075295]

Stute C, Schimmelpfeng K, Renkawitz-Pohl R, Palmer RH, and Holz A (2004). Myoblast determination in the somatic and visceral mesoderm depends on Notch signalling as well as on milliways (miliAlk) as receptor for jeb signalling. Development 131, 743–754. [PubMed: 14757637]

Sun J, and Stathopoulos A (2018). Fgf controls epithelial-mesenchymal transitions during gastrulation by regulating cell division and apicobasal polarity. Development 145, dev161927. [PubMed: 30190277]

Sutherland D, Samakovlis C, and Krasnow MA (1996). branchless encodes a *Drosophila* FGF homolog that controls tracheal cell migration and the pattern of branching. Cell 87, 1091–1101. [PubMed: 8978613]

Tanentzapf G, Devenport D, Godt D, and Brown NH (2007). Integrin-dependent anchoring of a stem-cell niche. Nat. Cell Biol 9, 1413–1418. [PubMed: 17982446]

Tepass U, and Hartenstein V (1994). Epithelium formation in the *Drosophila* midgut depends on the interaction of endoderm and mesoderm. Development 120, 579–590. [PubMed: 8162857]

Tulina N, and Matunis E (2001). Control of stem cell self-renewal in *Drosophila* spermatogenesis by JAK-STAT signaling. Science 294, 2546–2549. [PubMed: 11752575]

Vassilev V, Platek A, Hiver S, Enomoto H, and Takeichi M (2017). Catenins steer cell migration via stabilization of front-rear polarity. Dev. Cell 43, 463–479.e5. [PubMed: 29103954]

Voog J, D'Alterio C, and Jones DL (2008). Multipotent somatic stem cells contribute to the stem cell niche in the *Drosophila* testis. Nature 454, 1132–1136. [PubMed: 18641633]

Wang C, Chen J, Wen P, Sun P, and Xi R (2016). Chapter 2. Stem cell niche. In Regenerative Medicine—from Protocol to Patient: 1. Biology of Tissue Regeneration, Third Edition, Steinhoff G, ed. (Springer International Publishing), pp. 57–85.

Weiss JB, Suyama KL, Lee HH, and Scott MP (2001). Jelly belly: a *Drosophila* LDL receptor repeat-containing signal required for mesoderm migration and differentiation. Cell 107, 387–398. [PubMed: 11701128]

Weyers JJ, Milutinovich AB, Takeda Y, Jemc JC, and Van Doren M (2011). A genetic screen for mutations affecting gonad formation in *Drosophila* reveals a role for the slit/robo pathway. Dev. Biol 353, 217–228. [PubMed: 21377458]

Xiao T, Staub W, Robles E, Gosse NJ, Cole GJ, and Baier H (2011). Assembly of lamina-specific neuronal connections by Slit bound to type IV Collagen. Cell 146, 164–176. [PubMed: 21729787]

Yamashita YM, Jones DL, and Fuller MT (2003). Orientation of asymmetric stem cell division by the APC tumor suppressor and centrosome. Science 301, 1547–1550. [PubMed: 12970569]

Yamashita YM, Mahowald AP, Perlin JR, and Fuller MT (2007). Asymmetric inheritance of mother versus daughter centrosome in stem cell division. Science 315, 518–521. [PubMed: 17255513]

Yang L, Garbe DS, and Bashaw GJ (2009). A frazzled/DCC-dependent transcriptional switch regulates midline axon guidance. Science 324, 944–947. [PubMed: 19325078]

Zaffran S, Küchler A, Lee HH, and Frasch M (2001). *biniou* (FoxF), a central component in a regulatory network controlling visceral mesoderm development and midgut morphogenesis in *Drosophila*. Genes Dev. 15, 2900–2915. [PubMed: 11691840]

Highlights

- Slit and FGF signals from Vm are required for testis niche assembly
- Niche cells express the transcription factor *islet* in response to assembly cues
- *islet* is required for niche cytoskeletal polarity and anterior assembly
- Testis niche assembly is required for its function

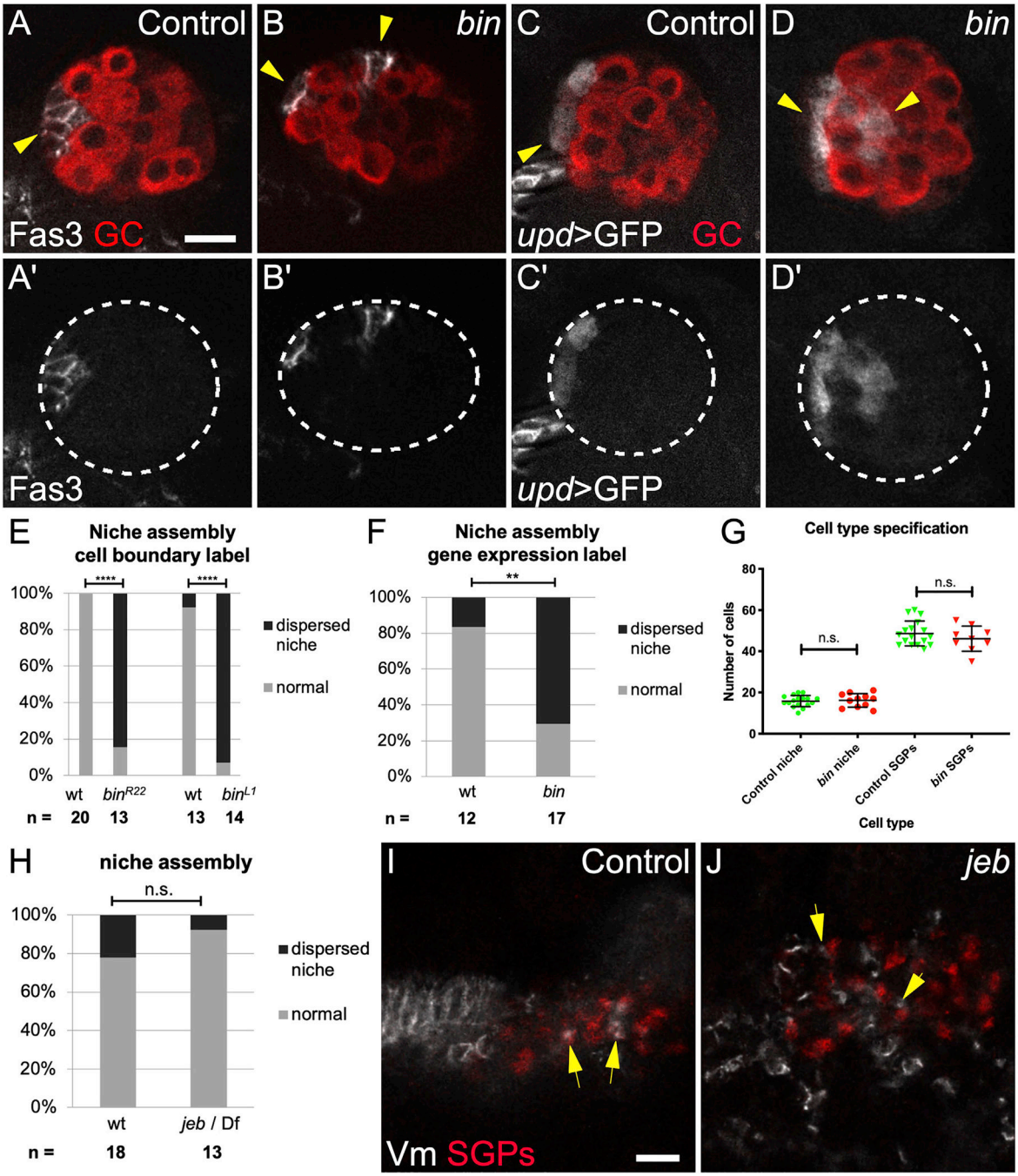

Figure 1. Visceral mesoderm is required for niche assembly and positioning

(A) Control Stage 17 gonad when niche morphogenesis is complete, immunostained with Vasa (red, germ cells) and Fas3 (white, niche cells, arrow).

(B) *biniou* mutant; Vasa (red) and Fas3 (white) reveal a dispersed niche (arrowheads).

(C) Control and (D) *biniou* mutant gonads immunostained with Vasa (red) and expressing *upd*-Gal4, UAS-GFP in niche cells (white, arrow).

(A′ and B′) Fas3 alone; (C′ and D′) GFP alone. Dotted lines, gonad boundary.

(E and F) Quantification using (E) Fas3 or (F) *upd* > GFP as marker ($p < 0.001$, $p = 0.004$, respectively, Fisher's exact test).
(G) Number of niche and non-niche SGPs specified in *biniou* mutants compared with siblings.
(H) Niche assembly is not affected in *jeb* mutants compared with siblings.
(I) Control and (J) *jeb* mutant embryos (Stage 13, before gonad coalescence); arrows show SGPs (Traffic jam, red) in contact with Vm cells (Fas3, white). *Jeb* mutants have a different arrangement of Vm precursors. Scale bars, 10 μm.

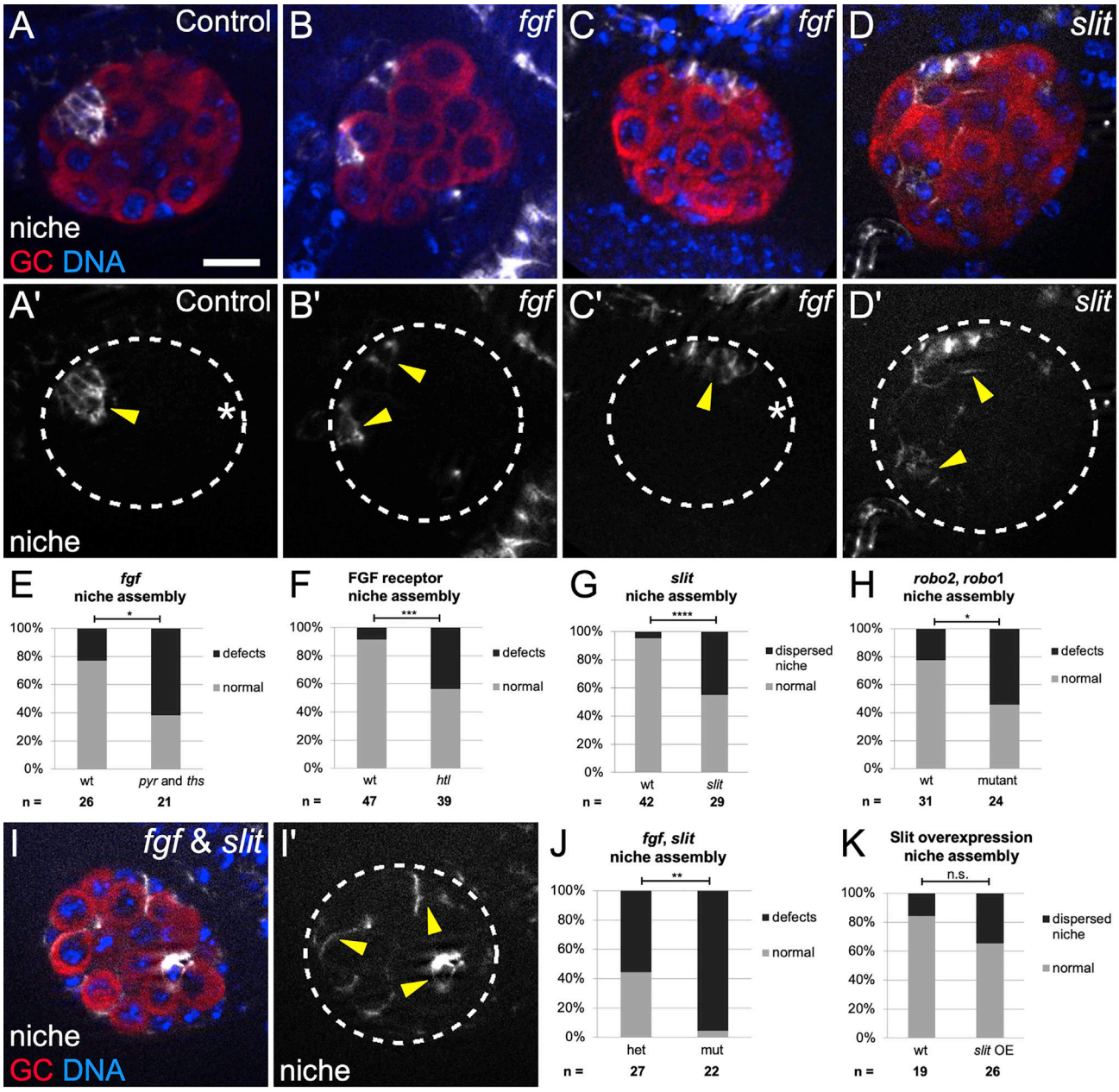

Figure 2. Slit and FGF signaling promote anterior niche assembly

(A–D and I) Stage 17 gonads, merge of Vasa (red, germ cells), Hoechst (blue, DNA), and Fas3 (white, niche cells), or single channel (Fas3); dotted line, gonad boundary. Scale bars, 10 μm. Prime panels show Fas3 (niche cells, arrowheads) alone.

(A) Sibling controls have a single, anterior niche.

(B and C) Df(2R)BSC25 gonads, with a deletion removing *pyr* and *ths* genes, exhibit niche defects such as (B) dispersed niche cell aggregates and (C) niches not at the gonad anterior (asterisk, gonad posterior).

(D) *slit[2]* mutant gonads often have dispersed niche cell aggregates.

(E–H) Quantification of niche defects (Fisher's exact test), (E) with *pyr* and *ths* removed (*fgf*) ($p = 0.016$), (F) FGF *htl* receptor mutant ($p = 0.0003$), (G) *slit* mutant ($p < 0.0001$), and (H) *robo2*, *robo1* double mutant ($p = 0.024$).

(I and J) Combined mutant with *slit*, and *pyr* and *ths* removed (*fgf*) exhibit dispersed niche cells ($p = 0.003$).

(K) Niche morphogenesis defects were not significant (n.s.) in Slit overexpression embryos.

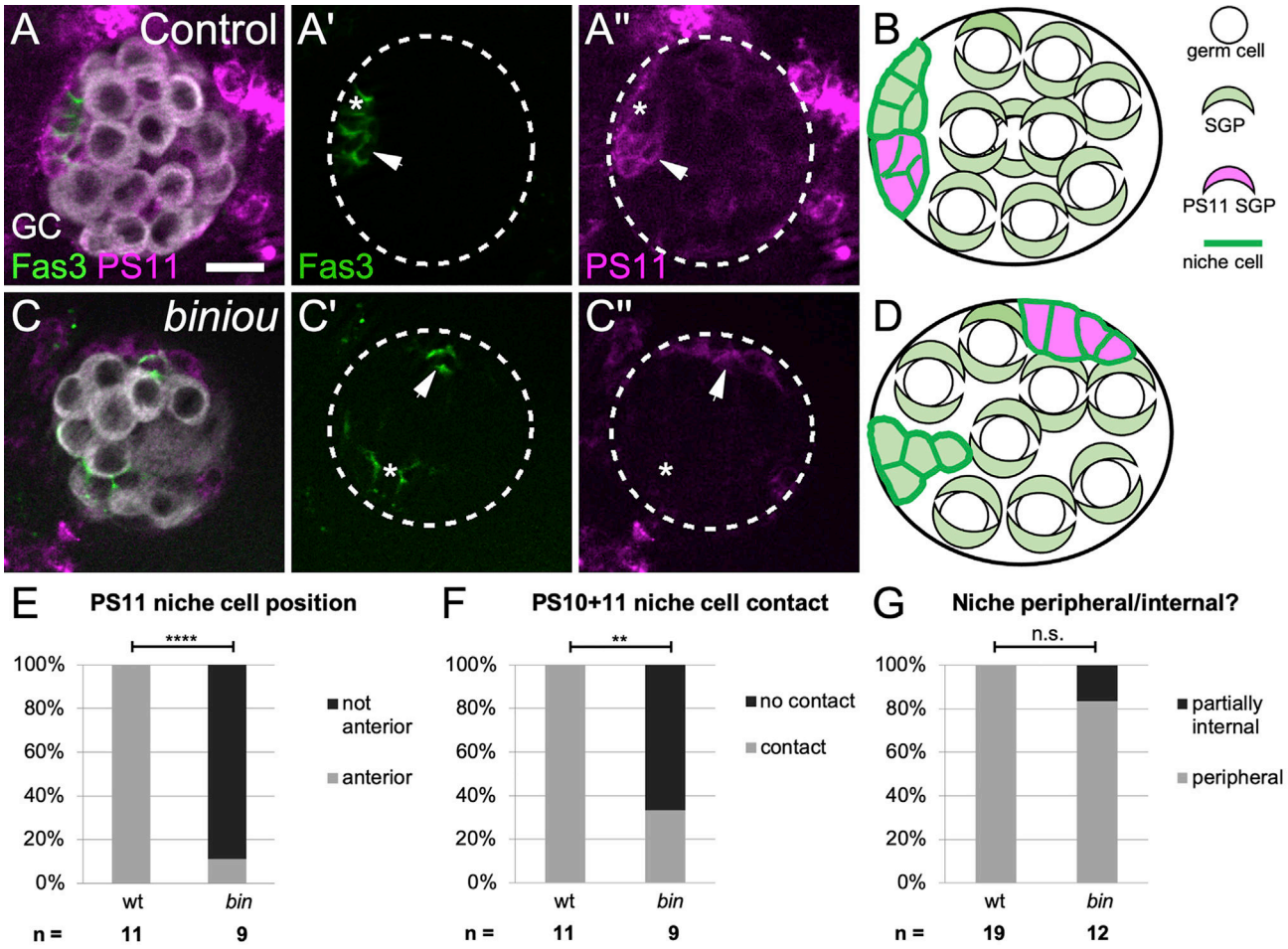

Figure 3. *biniou* is required for anterior movement of pro-niche cells

(A and C) Stage 17 gonads expressing mcd8GFP in PS11 cells (magenta), and immunostained with Vasa (white, germ cells) and Fas3 (green, all niche cells). (A) A control, with a single anterior niche (left, green) containing cells deriving from both PS 10 (A′, green alone, asterisk) and PS 11 (A′ and A′′, magenta and green, arrow). (C) *biniou* mutant with dispersed niche cell aggregates (green). Anterior niche cells deriving from PS 10 (C′, green alone, asterisk) do not associate with PS 11-derived niche cells (C′′, magenta and green, arrows). Ectopic PS11 niche cells were distinguishable from PS13 msSGPs, which do not express the niche cell marker Fas3.

(B and D) Cartoons illustrating the distribution of PS11 niche cells in (B) control and (D) *biniou* mutants.

(E–G) Quantifications comparing *biniou* mutants and sibling controls (Fisher's exact test) by how often (E) PS 11-derived niche cells are located at anterior ($p < 0.0001$), (F) PS 11 niche cells contact anterior PS 10 niche cells ($p < 0.0022$), and (G) niche cells are located within 2 μm of the gonad periphery. Scale bars, 10 μm.

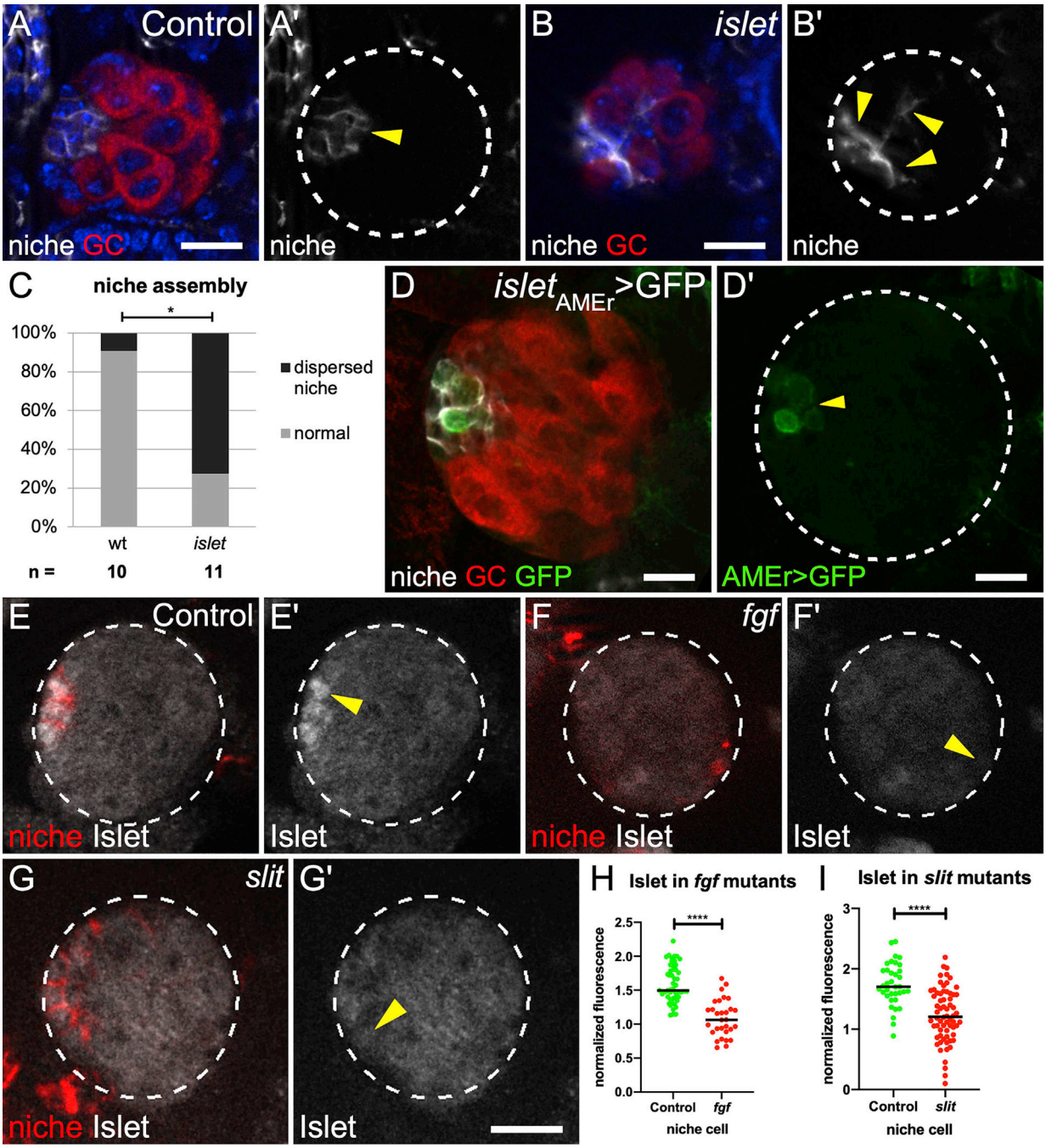

Figure 4. *islet* is expressed in niche cells in response to Vm signals

(A and B) (A) Control and (B) *islet* mutant Stage 17 gonads immunostained with Vasa (red, germ cells), Fas3 (white, niche cells), and Hoechst (blue, nuclei). (A′ and B′) Fas3 alone (arrows).

(C) Quantification of niche assembly in *islet* versus sibling controls ($p = 0.024$, Mann-Whitney test).

(D) St 17 gonad expressing GFP driven by the *islet* AMEr enhancer stained with Vasa (germ cells, red) and Fas3 (niche cells, white). (D′) *islet* AMEr-driven GFP alone.

(E–G) Stage 17 gonads immunostained for Islet (white), Fas3 (red, niche cells), and Vasa (not shown, germ cells). Gonad boundaries, dotted lines. Arrowheads, niche cells. (E′–G′) Islet alone.

(H and I) Islet accumulation in niche cells from (H) *pyr* and *ths* removed (*fgf*) and (I) *slit* mutants, compared with sibling controls ($p < 0.0001$, Mann-Whitney test). Scale bars, 10 μm.

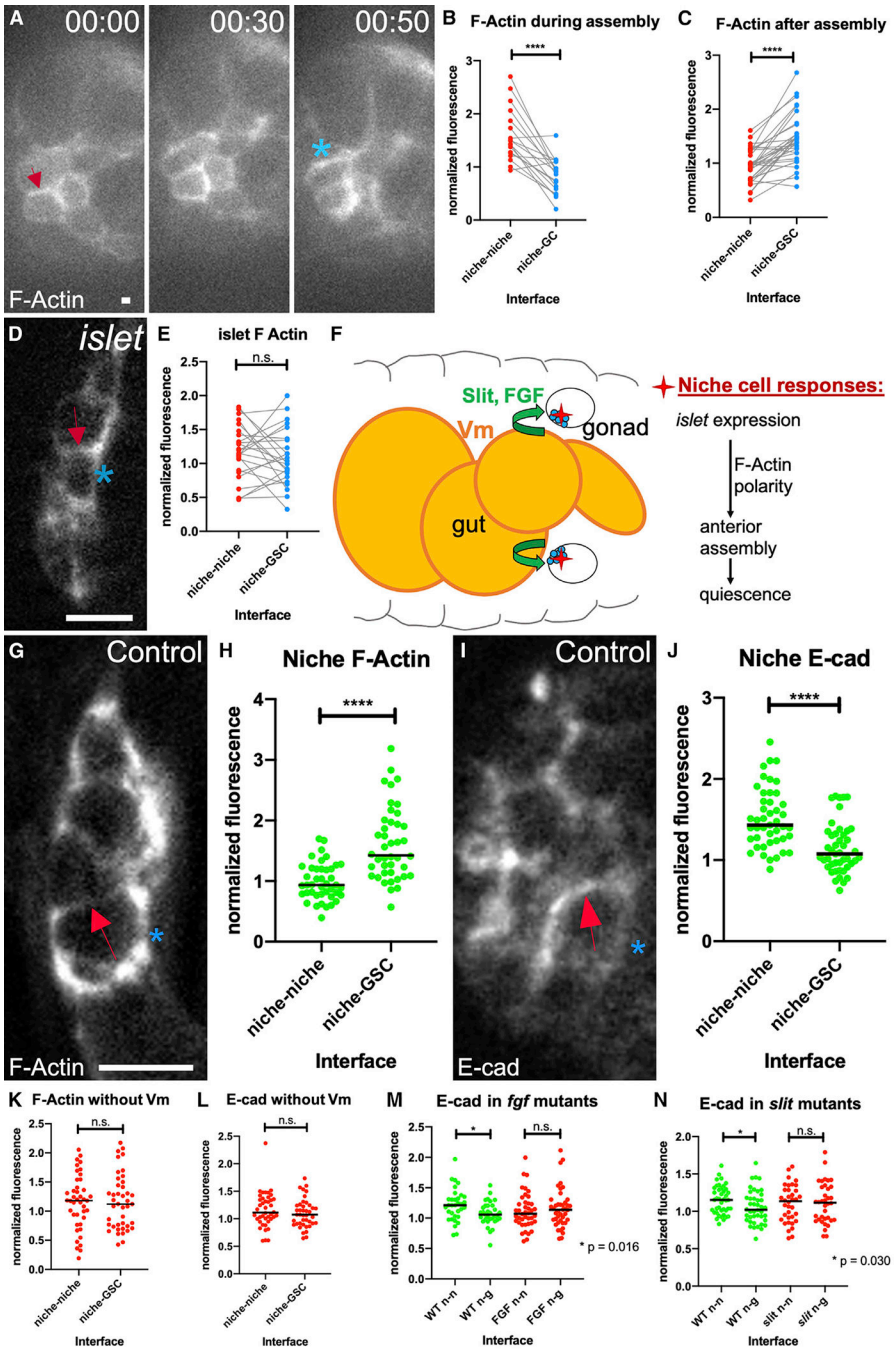

Figure 5. Niche cells are polarized during assembly

(A) Stills from a time course of a gonad expressing *six4*-eGFP::moesin to label F-actin in all SGPs. F-actin accumulates at niche-niche interfaces when niche cells begin to associate (arrow), and later repolarizes to niche-stem cell interfaces (asterisk).

(B and C) Quantification of F-actin accumulation at niche-niche or niche-germ cell interfaces (B) during and (C) after completion of niche assembly in fixed tissue ($p < 0.0001$, Wilcoxon test).

(D) Niche cells in fixed tissue expressing a somatic cell F-actin label, *six4*-eGFP::moesin in *islet* mutants in which niche cells have begun to associate but have not completed assembly.
(E) F-actin accumulation at niche cell interfaces in *islet* mutants.
(F) A model illustrating how Vm signals influence niche assembly.
(G and I) Niche cells from fixed Stage 17 control gonads (G) expressing *six4*-eGFP::moesin or (I) immunostained for E-cadherin.
(H) F-actin accumulation at niche-GSC interfaces versus niche-niche interfaces ($p < 0.0001$, Mann-Whitney test).
(J) E-cadherin accumulates at niche-niche interfaces compared with niche-GSC interfaces ($p < 0.0001$, Mann-Whitney test).
(K–N) Quantification of polarity loss in Stage 17 niches for (K) F-actin in *biniou*, (L) E-cadherin in *biniou*, (M) Ecad with *pyr* and *ths* removed (*fgf*), or (N) Ecad in *slit* mutants (Mann-Whitney tests). Asterisks, niche-GSC interfaces; arrows, niche-niche interfaces. Scale bars, 5 μm.

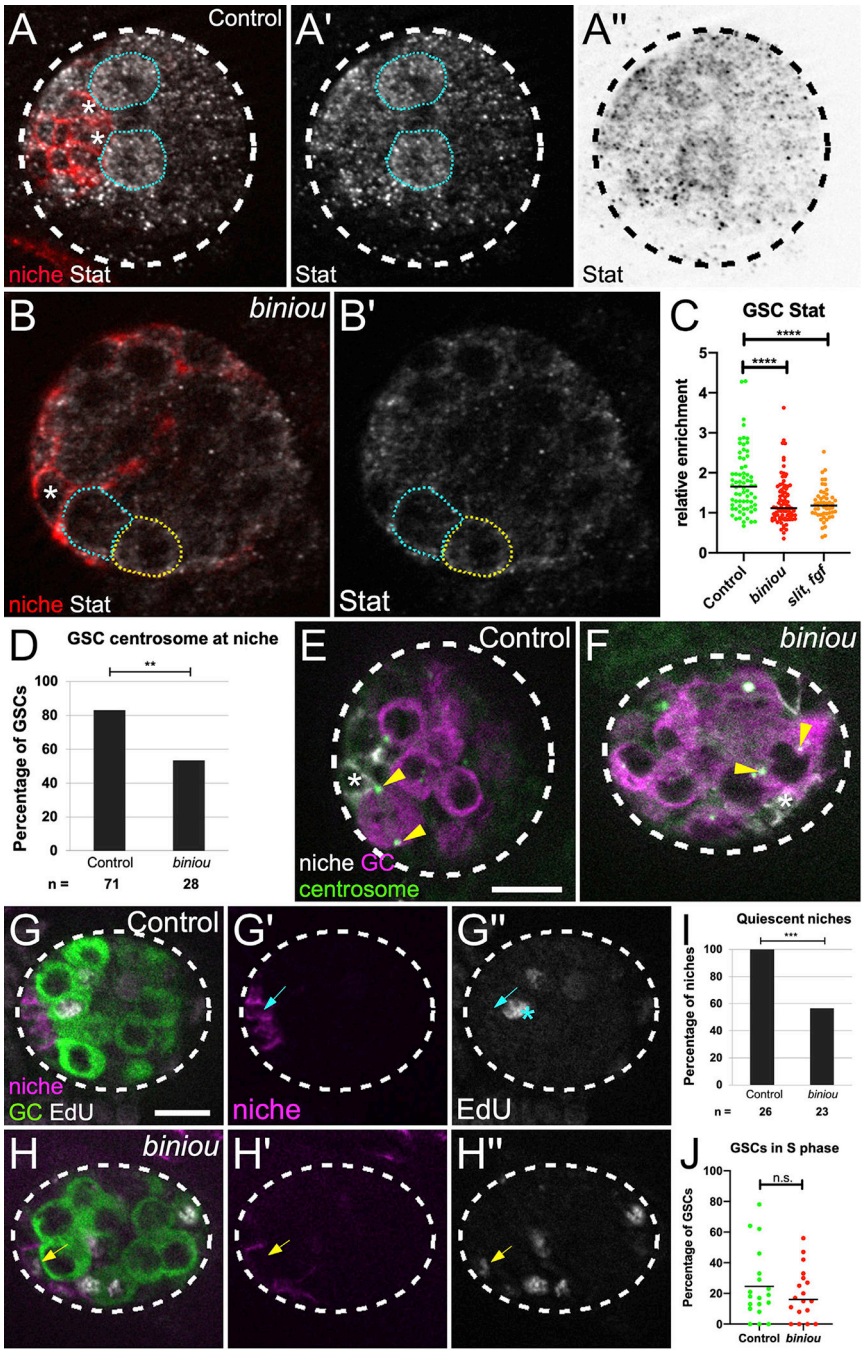

Figure 6. Niche assembly is required for niche function

(A and B) Stage 17 gonad, Stat (white), Fas3 (red, niche cells), and Vasa (germ cells; not shown). Niche cell, asterisk; GSCs, blue dotted line; neighboring germ cells, yellow-dotted line. (A′ and B′) Stat alone. (A″) inverted Stat.

(C) Stat accumulation in GSCs relative to neighboring germ cells in control, *biniou* or combined signaling mutant (*slit*, *pyr*, and *ths*).

(D) Quantification of control versus *biniou* mutants for percentage of GSCs with a centrosome at a GSC-niche interface (p = 0.004, Fisher's exact test).

(E and F) Stage 17 gonad, γ-tubulin (green, centrosomes), Fas3 (white, niche cells), and Vasa (magenta, germ cells). Arrowheads, GSC centrosomes; asterisk, adjacent niche cell. (G and H) Stage 17 gonads pulsed with EdU, fixed and immunostained. Merge shows EdU (white), Fas3 (magenta, niche), and Vasa (green, germ cell), along with single channel Fas3 (G′ and H′), and EdU (G″ and H″). (G′) Control niche cell with no EdU incorporation (blue arrow), and (H′) a *biniou* mutant niche cell incorporating EdU (yellow arrow). Asterisk, S phase GSC.

(I and J) Quantification of control versus *biniou* mutants for: (I) percentage of gonads with quiescent niches ($p = 0.0001$, Fisher's exact test); (J) S-phase index of GSCs. Scale bars, 10 μm.

KEY RESOURCES TABLE

REAGENT or RESOURCE	SOURCE	IDENTIFIER
Antibodies		
Rabbit polyclonal anti Vasa	R. Lehmann	N/A
Goat polyclonal anti Vasa	Santa Cruz Biotechnology	Cat# sc-26877 (dC-13), RRID:AB_793880 Discontinued
Mouse monoclonal anti Fasciclin III	Developmental Studies Hybridoma Bank	DSHB:7G10; RRID:AB_528238
Rabbit polyclonal anti STAT92E	E. Bach	N/A
Rabbit polyclonal anti RFP	Abcam	ab62341; RRID:AB_945213
Mouse monoclonal anti Islet	Developmental Studies Hybridoma Bank	DSHB:40.3A4; RRID:AB_528313
Rat monoclonal anti DE-cadherin	Developmental Studies Hybridoma Bank	DSHB:DCAD2 RRID: AB_528120
Guinea pig polyclonal anti Traffic jam	D. Godt	N/A
Mouse monoclonal anti Gamma Tubulin	Sigma	GTU-88, T6557
Chick polyclonal anti GFP	Aves labs	Cat#GFP-1020; RRID: AB_2307313
Rabbit polyclonal anti Biniou	E. Furlong	N/A
Normal Donkey Serum (NDS)	Jackson Immunoresearch Laboratories	Cat#: 017-000-121; RRID: AB_2337258
Alexafluor Secondary Antibodies (488, 647)	Molecular Probes	N/A
Cy3 Affinipure Secondary Antibodies	Jackson ImmunoResearch	Cat#: 711-165-152; RRID: AB_2307443
Chemicals, peptides, and recombinant proteins		
Para-Formaldehyde (PFA), 16%	Electron Microscopy Sciences	Cat#15710
Hoechst	Sigma	Cat#33342; CAS Number: 875756-97-1
Propyl-gallate	Propyl-gallate	SKU: P3130; CAS Number 121-79-9; PubChem Substance ID 24898394
Normal Donkey Serum (NDS)	Jackson Immunoresearch Laboratories	017-000-121; RRID: AB_2337258
Normal Goat Serum (NGS)	Jackson Immunoresearch Laboratories	Jackson Immunoresearch Laboratories
Ringer's solution	Other	https://doi.org/10.1101/pdb.rec12409
Critical commercial assays		
Click-iT EdU	ThermoFisher	Cat#: C10419
Experimental models: Organisms/strains		
six4-nls-eGFP	D. Finnegan	Clark et al., 2006
P-Dsix4-eGFP::Moesin	R. Lehmann	Sano et al., 2012
nos-moesin::GFP	R. Lehmann	Sano et al., 2005; FBtp0040584
His2Av::mRFP1	Bloomington Drosophila Stock Center	FBtp0056035
Prd-Gal4	Bloomington Drosophila Stock Center	FBst0001947
tupAME-Gal4	J.-L. Frendo	N/A
UAS-tdTomato	Bloomington Drosophila Stock Center	FBst0036328
trh8 / TM3, twi-Gal4, UAS-GFP	D. Andrew	FBal0050667
y1 w*; tup1 P{neoFRT}40A / CyO	Bloomington Drosophila Stock Center	FBst0036503; RRID:BDSC_36503
tupex4	S. Campuzano	FBal0216723

REAGENT or RESOURCE	SOURCE	IDENTIFIER
TM3, P{w[+mC]=GAL4-twi.G}2.3, P{UAS-2xEGFP}AH2.3, Sb[1] Ser[1]	Bloomington Drosophila Stock Center	FBst0006663; RRID:BDSC_6663
w1118	Bloomington Drosophila Stock Center	BL#3605; RRID:BDSC_3605
upd-Gal4	E. Matunis	N/A
biniou[R22}	M. Frasch	Zaffran et al., 2001; FBal0043738
biniou[I1]	M. Frasch	Zaffran et al., 2001; FBal0043737
UAS-mcd8GFP	Bloomington Drosophila Stock Center	FBtp0002652
jeb[weli]	A. Holz	Stute et al., 2004; FBal0159133
Df(2R)BSC699	Bloomington Drosophila Stock Center	FBab0045764
Df(2R)BSC25	Bloomington Drosophila Stock Center	FBab0029944
slit[2]	Bloomington Drosophila Stock Center	Battye et al., 1999; FBal0015700
htl[AB42]	Bloomington Drosophila Stock Center	FBal0057264
hlh54f[delta598]	Ismat et al., 2010	FBal0248839
twi-Gal4	Bloomington Drosophila Stock Center	FBtp0000706
UAS-*sli.D*	Bloomington Drosophila Stock Center	FBti0186586
UAS-*ths*289.22	A. Stathopoulos	Kadam et al., 2012
pyr-Gal4	Bloomington Drosophila Stock Center	FBti0212964; Lee et al., 2018. A gene-specific T2A-GAL4 library for Drosophila. eLife 7:e35574
ths-Gal4	Bloomington Drosophila Stock Center	FBti0196141; Wu et al., 2017. Fibroblast growth factor signaling instructs ensheathing glia wrapping of Drosophila olfactory glomeruli. PNAS 114: 7505-7512
UAS-red Stinger	Bloomington Drosophila Stock Center	FBti0040830
Htl-mCherry	A. Stathopoulos	Irizarry and Stathopoulos, 2015
robo2[X123]	G. Bashaw	FBal0123720
robo1[GA285]	G. Bashaw	FBal0032588
slit-LacZ	Bloomington Drosophila Stock Center	FBti0006990
Slit::GFP	Bloomington Drosophila Stock Center	FBti0181864
Recombinant DNA		
GAA GAA TCC CAG CAA AGA CCG TGA GTTG	Clark et al., 2006	D-six4 third intron, forward, EcooRI site
GTT GGA TCC ATT GCC ATC CAG TTG	Clark et al., 2006	D-six4 third intron, reverse, BamH1 site
Software and algorithms		
FIJI (Image J)	www.fiji.sc	N/A
Image J	www.imagej.nih.gov/ij/	N/A
Metamorph Microscopy Automation and Image Analysis Software	Leica;https://www.moleculardevices.com/products/cellular-imaging-systems/acquisition-and-analysis-software/metamorph-microscopy	v7.8.40; RRID:SCR_002368
Axio-Vision Imaging Software	Zeiss	v4.8.1
Adobe Photoshop	https://www.adobe.com/uk/products/photoshop.html	RRID:SCR_014199
Graphpad Prism	Graphpad Software	v7.0; RRID:SCR_002798

REAGENT or RESOURCE	SOURCE	IDENTIFIER
Other		
Matek imaging dish	Thermofisher	P35G-1.5-14-C
Leica DM16000 B inverted spinning disk confocal	Leica	N/A
63x / 1.2 NA water immersion objective	Leica	506279
40x / 1.1 NA water immersion objective	Leica	N/A
Leica M165FC	Leica	N/A
Leica M165C	Leica	N/A
GFP Filter set ET470/40x; ET525/50m	Leica 10447408	N/A
mCherry Filter set ET560/40x; ET630/75m	Leica 10450195	N/A
DAPIFilter set AT350/50x; ET460/50m	Leica 10450196	N/A
Achromat 1.6x objective	Leica 10450163	N/A
Video 0.63x objective	Leica 10447367	N/A
Needle holder	Fisher Scientific	N/A
Nytex basket		N/A